Supporting Information

Digital light processing (DLP) 3D-fabricated antimicrobial hydrogel with a sustainable resin of methacrylated woody polysaccharides and hybrid silver-lignin nanospheres

Luyao Wang,[a] Qingbo Wang,[a] Anna Slita,[b] Oskar Backman,[a] Zahra Gounani,[c] Emil Rosqvist,[d] Jouko Peltonen,[d] Stefan Willför,[a] Chunlin Xu,[a] Jessica M. Rosenholm,[b] and Xiaoju Wang [*a,b]

17 pages, 11 Figures, 9 Tables

[a] Laboratory of Natural Materials Technology, Faculty of Science and Engineering, Åbo Akademi University, Henrikinkatu 2, Turku FI-20500, Finland

[b] Pharmaceutical Sciences Laboratory, Faculty of Science and Engineering, Åbo Akademi University, Tykistökatu 6A, Turku FI-20520, Finland

[c] Physics, Åbo Akademi University, Henrikinkatu 2, Turku FI-20500, Finland

[d] Laboratory of Molecular Science and Engineering, Faculty of Science and Engineering, Åbo Akademi University, Henrikinkatu 2, Turku FI-20500, Finland

*Corresponding author email address: Xiaoju.Wang@abo.fi

Characterizations

Transmission electron microscopy (TEM): The morphology of LNP and LNP@Ag were analyzed by a TEM microscope (JEM-1400 PLUS, JEOL Ltd., Japan) in bright-field mode with an accelerating voltage of 80 kV. A dispersion of LNP or LNP@Ag was prepared in distilled water at a concentration of 0.01 wt%, and 5 µL of the dispersion was dropped onto a copper grid (200 mesh, TED PELLA INC. USA) coated with thin carbon film and then incubating at ambient temperature for 3 min. The excess liquid was removed by blotting with filter paper before loading in the TEM microscope. The average particle size of LNP and AgNPs was measured by imaging 150 - 200 particles from TEM images using Image J software.

Hydrodynamic diameter and ζ-potential analysis: The intensity weighted average hydrodynamic diameter (Z-average), polydispersity index (PDI) by intensity, and surface charge (ζ-potential) of the as-synthesized LNP and LNP@Ag were determined by using a Zetasizer Nano instrument (Malvern Instruments). The samples for dynamic light scattering (DLS) and ζ-potential measurements were prepared in distilled water at a concentration of around 0.2 $mg.mL^{-1}$ and analyzed at 25 °C. DLS measurement parameters were as follows: a Helium-Neon laser wavelength of 632.8 nm; a scattering angle of 173°; the refractive index (RI) and viscosity of the dispersant (distilled water) were set to be 1.324 and 0.887 x 10^{-3} pa.s, respectively; the RI and absorption value of the LNP@Ag were set to be 1.595 and 0.200 respectively, which were the same as those of LNP. The Z-average, PDI, and ζ-potential values were collected through three consecutive measurements, for which the mean result was reported.

FTIR analysis: The infrared (IR) absorbance of the samples (i.e., LNP and LNP@Ag freeze-dried powders) were measured with a Fourier-transform infrared spectroscopy (FTIR) (Nicolet iS50 FT-IR Spectrometer, ThermoFisher Scientific™) equipped with a standard sample compartment and a sample holder. All the samples for FTIR measurements were prepared by uniformly mixing 200 mg of potassium bromide (KBr) with 2 mg of sample in an agate mortar. Then the KBr/sample mixture was tableted and tested for FTIR analysis. Sixty-four scans for each sample were taken with a resolution of 4 cm^{-1} ranging from 4000 to 400 cm^{-1}.

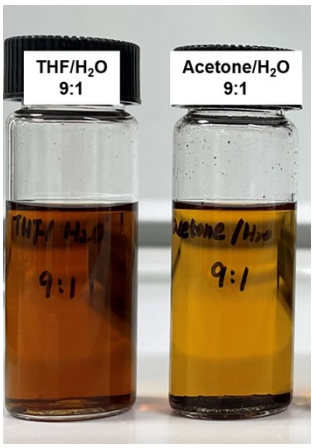

Fig. S1 Solubility of laccase-polymerized MeOH-s fraction (incubated with laccase for 4 hours) in THF/H_2O (9:1, v/v) and acetone/H_2O (9:1, v/v). The image was taken after 1 day of dissolution.

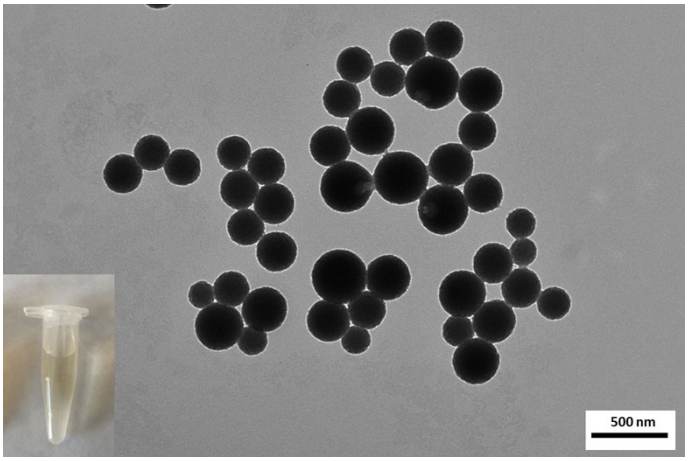

Fig. S2 TEM image of L-*i*-PrOH-LNP@Ag aqueous dispersion. The inset was the photograph of the LNP-$[Ag(NH_3)_2]^+$ aqueous dispersion over 4 hours reaction time.

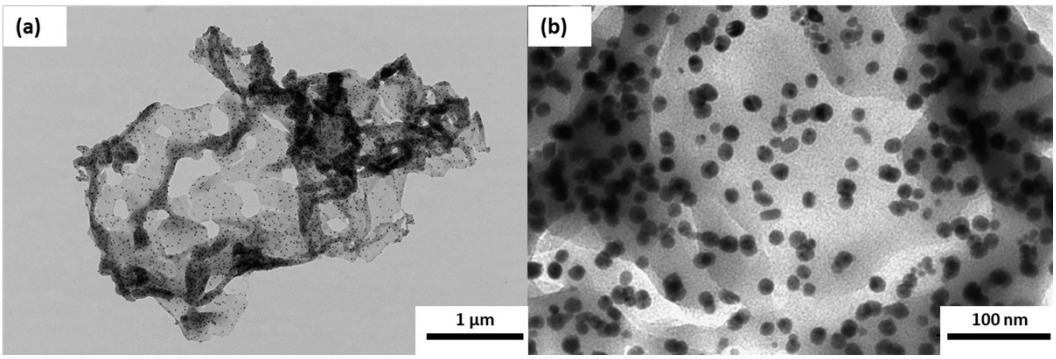

Fig. S3 TEM images of MeOH-LNP@Ags used as a representative sample to show the deficient alkali resistance of lignin without polymerization but possess the capacity to reduce Ag^+. The preparation process for MeOH-LNP@Ag was the same as LM-4-NP@Ag.

XPS analysis of the LNP and LNP@Ag

The high-resolution XPS spectra of LNP and LNP@Ag are shown in **Fig. S4**. The detailed deconvolution of the core-level regions of C 1s and O 1s, including the band binding energies and relative area percentages were listed in **Table S3.** No significant binding energy shifts were found in the deconvoluted bands from C 1s and O 1s core-level regions after the incorporation of AgNPs, whereas the band area did change. Briefly, the relative area percentages of C_2 (C-O/C-OH) and O_2 (C-O-C/C-OH) in LM-4-NP@Ag decreased compared with the LM-4-NP sample. Meanwhile, the relative area percentages of C_3 (O-C-O/C=O), C_4 (O-C=O), and O_1 (C=O/C=O*-O) concomitantly increased. These changes all indicate the oxidation of lignin hydroxyl groups to carbonyl/carboxyl groups during the silver reduction.

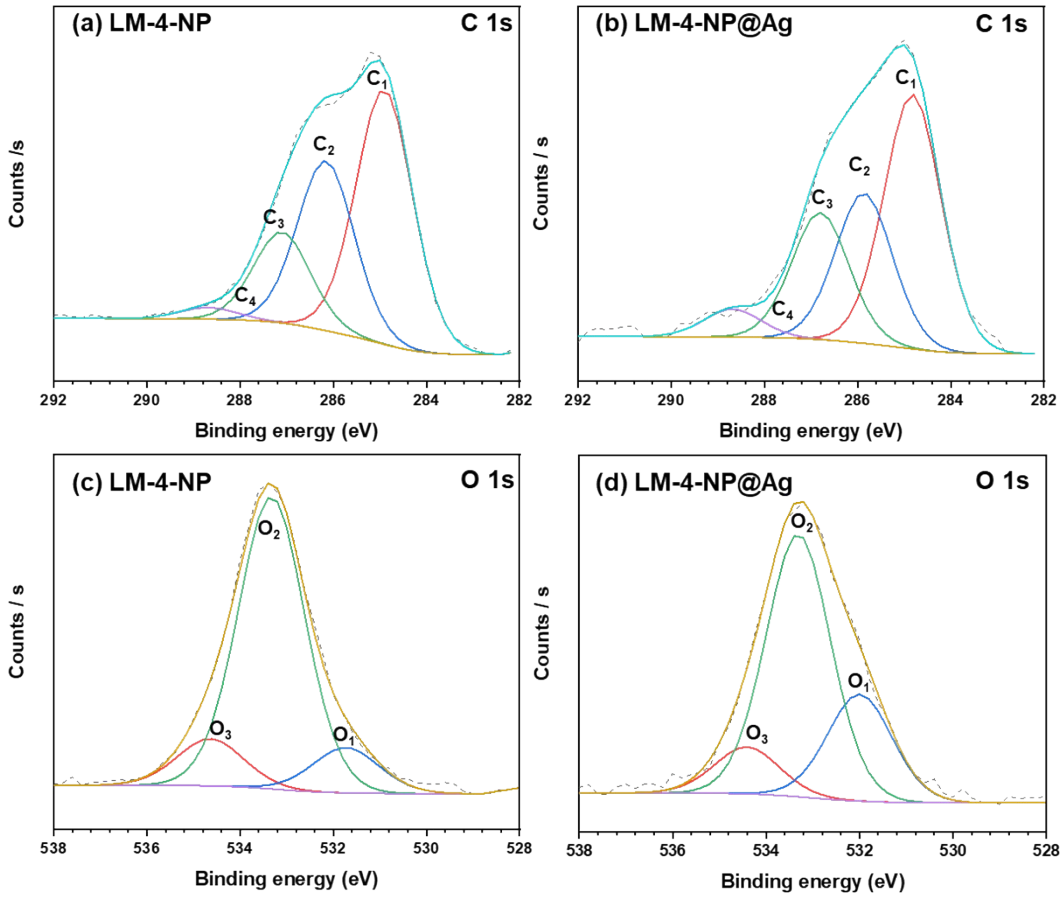

Fig. S4 High-resolution XPS spectra over C 1s and O 1s core-level regions of the (a) (c) LNP and (b) (d) LNP@Ag from laccase-polymerized MeOH-s lignin.

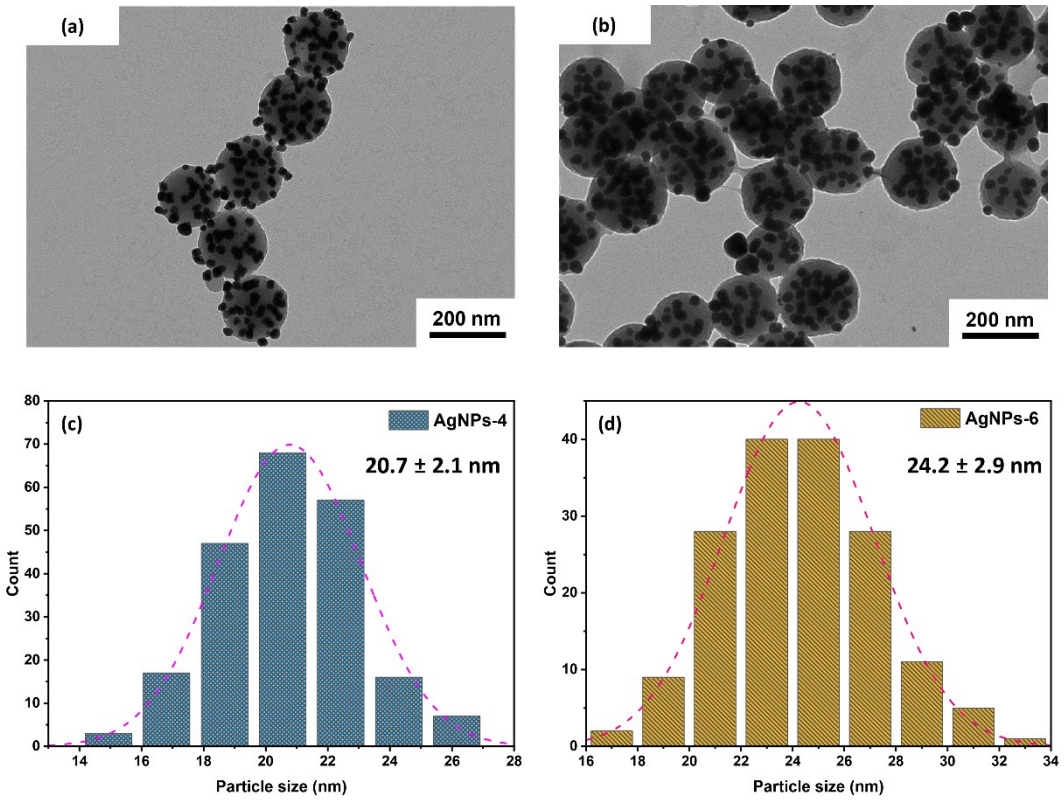

Fig. S5 TEM images of LM-4-NPs@Ag that reacted with $Ag(NH_3)_2NO_3$ (10 mg. mL^{-1}) for (a) 4 hours and (b) 6 hours, and their corresponding histogram (c-d) of particle diameter size distribution of AgNPs. Note: The TEM magnification in (a) and (b) was 40,000×.

FTIR analysis of the LNP and LNP@Ag

To ascertain the oxidation of lignin by silver, the chemical composition of LM-4-NP and LM-4-NP@Ag were analyzed by FTIR spectroscopy. All the characteristic absorptions related to the aromatic skeleton of lignin were observed in LNP and LNP@Ag samples. In the carbonyl/carboxyl region of LM-4-NP@Ag, the peak at 1720 cm^{-1} belongs to the absorption of non-conjugated C=O stretching,[1] and the band intensity at 1720 cm^{-1} was obviously stronger than that of the original LM-4-NP. The C-H stretching vibration in aromatic methoxyl groups ($-OCH_3$) and in methyl and methylene groups of lignin side chains was observed at 2936 cm^{-1} and 2841 cm^{-1} in LM-4-NP, which decreased in intensity in LM-4-NP@Ag. Furthermore, the sharp peak observed at 1215 cm^{-1} in LM-4-NP belongs to the syringyl (S) ring breathing with C-O stretching,[2] which shifted to a higher wavenumber in the FTIR spectrum of L-M-4-LNP@Ag. These results confirm the oxidation of lignin with the formation of carbonyl/carboxyl and quinone groups during the reaction with $Ag(NH_3)_2NO_3$ solution. The above-mentioned changes were also observed in the FTIR spectrum of LB-4-NP/LB-4-NP@Ag and LE-4-NP/LE-4-NP@Ag samples. However, neither the peak position nor the peak intensity was changed for the LI-4-LNP sample after being incubated with $Ag(NH_3)_2NO_3$ solution for 4 hours, which is in agreement with the chemical inert property of laccase-treated *i*-PrOH fraction.

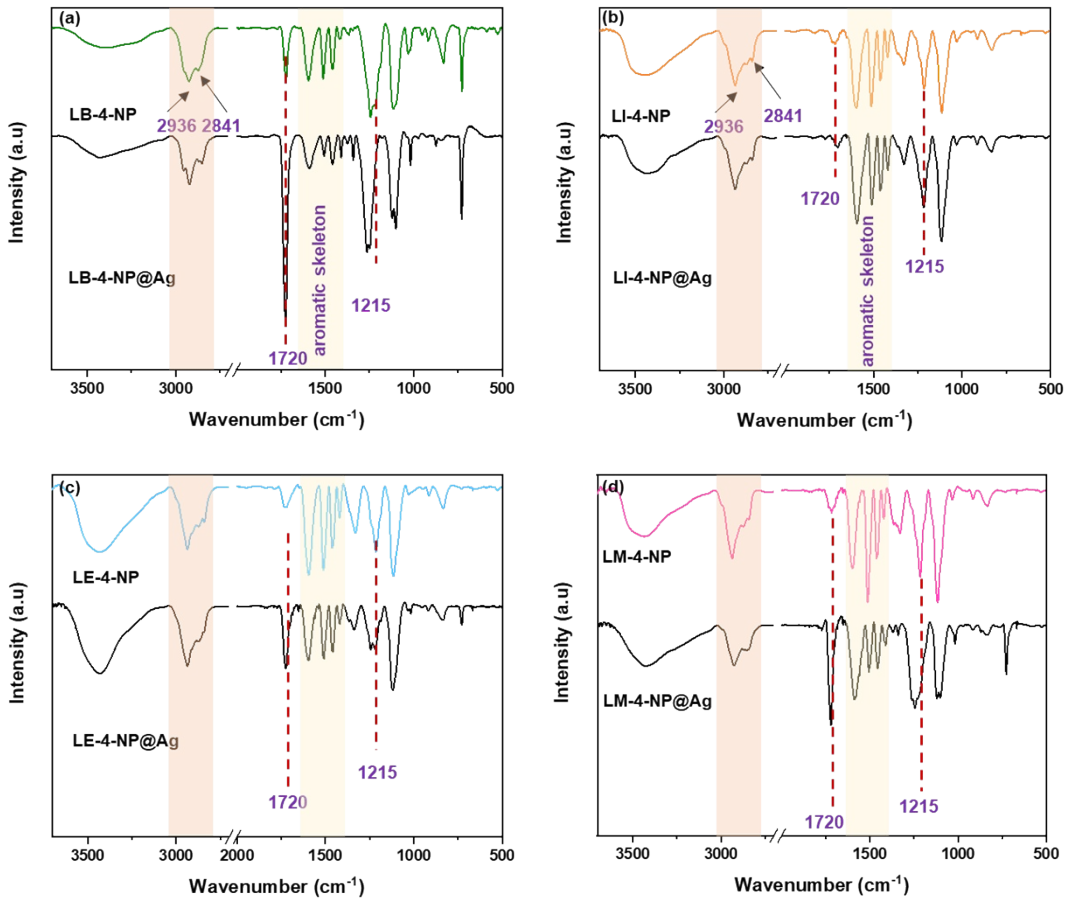

Fig. S6 FTIR spectra of the LNP and LNP@Ag prepared from (a) laccase-polymerized birch AL lignin, (b) laccase-polymerized *i*-PrOH-s lignin, (c) laccase-polymerized EtOH-s lignin, and (d) laccase-polymerized MeOH-s lignin.

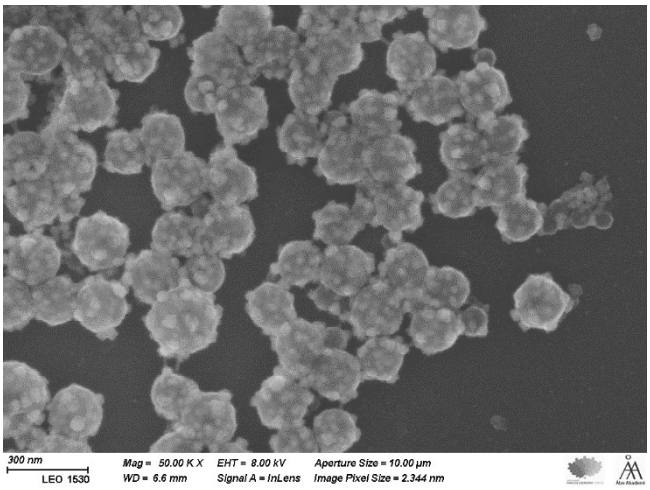

Fig. S7 SEM image of LM-4-NP@Ag powder.

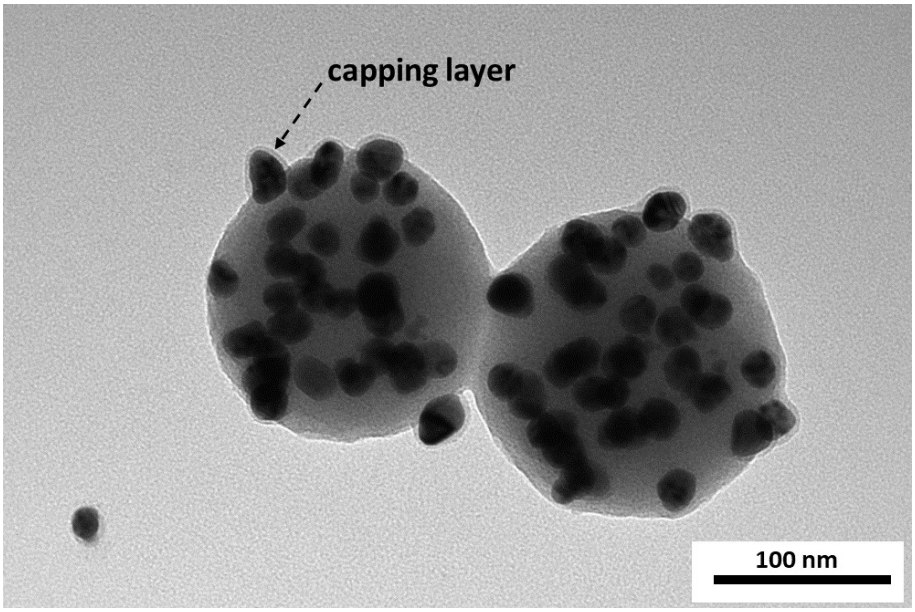

Fig. S8 TEM image of LM-4-NP@Ag showing the presence of lignin capping layer.

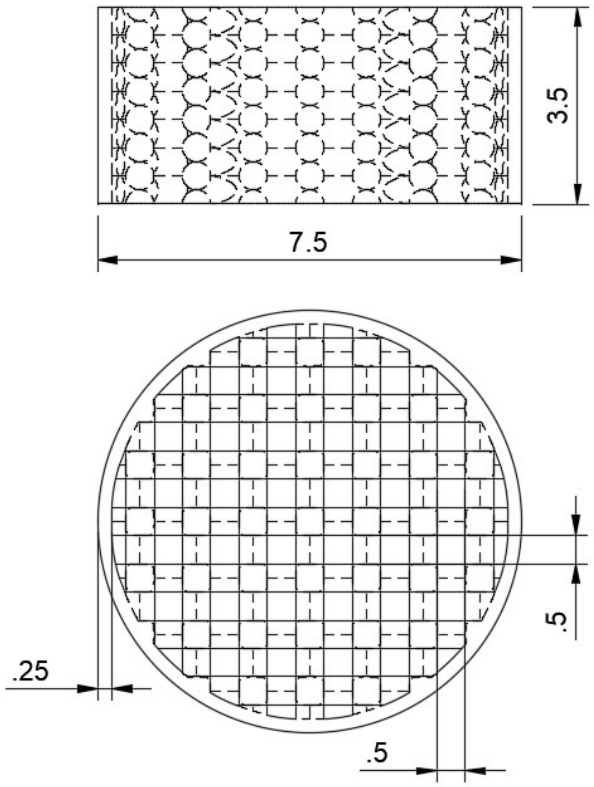

Fig. S9 The CAD drawing of the crosshatch scaffolds.

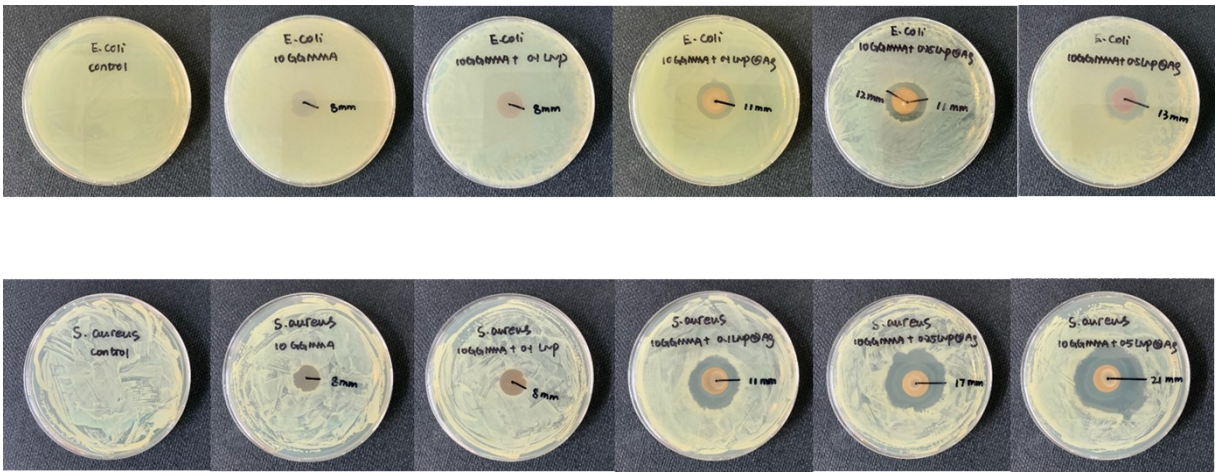

Fig. S10 Inhibition zone in disk diffusion test using GGMMA-based hydrogel (16 mm in diameter, 1 mm in thickness) discs cast by UV_{405}-LED.

Mass balance analysis

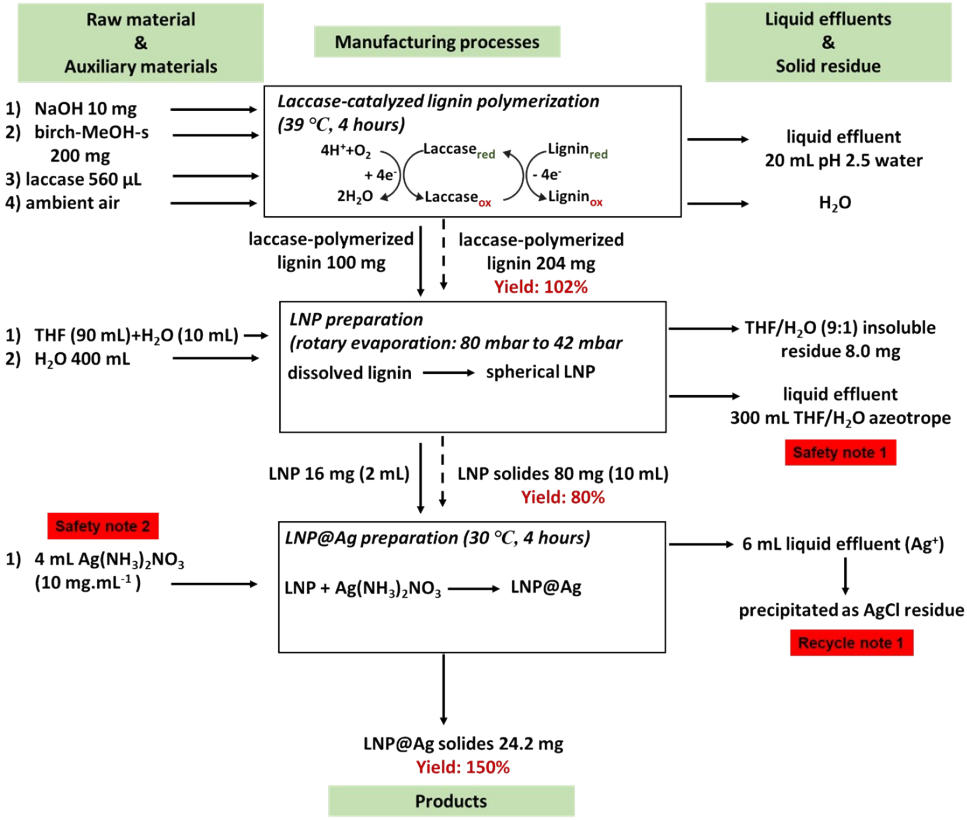

Fig. S11 Mass balance analysis of the laccase-catalyzed lignin polymerization and LNP as well as LNP@Ag preparation processes using LM-4-NP@Ag sample as a representative case.

Safety notes were addressed to the deployment of THF as the solvent for the LNP production and fresh preparation of $Ag(NH_3)_2NO_3$ and a **recycle note** was created for the precipitation of the residual Ag^+ as AgCl at the end of *in situ* AgNP generation on LNP.

Table S1. DLS results of the LNPs prepared from birch-MeOH-s fraction and laccase-polymerized MeOH lignin in aqueous media.

LNPs	hydrodynamic diameter[a]		dispersity[a]	
	Z-average (nm)	STDEV	PDI	STDEV
MeOH-NP	417.8	2.9	0.14	0.05
LM-1-NP[b]	290.1	5.0	0.15	0.03
LM-2-NP	242.1	1.3	0.12	0.04
LM-3-NP	216.1	2.5	0.12	0.01
LM-4-NP	167.0	2.6	0.11	0.01
LM-5-NP	143.5	1.0	0.24	0.02
LM-6-NP	117.9	1.9	0.28	0.02

[a]the results were obtained by calculating the average of three consecutive measurements. [b]LM-x-NP, x denotes the reaction time of lignin with laccase.

Table S2. UV-vis absorption bands and intensity of LM-4-NP@Ag dispersion in aqueous media.

reaction time (min)	lignin absorption intensity		SPR bands		relative intensity		
	289 nm	295.8 nm	wavelength (nm)	absorption intensity	289 nm /295.8 nm	SPR /289 nm	SPR / 295.8 nm
90	0.5518	0.5569	---[a]	---	0.9908	0	0
100	0.5408	0.5488	---	---	0.9853	0	0
120	0.5488	0.5573	---	---	0.9848	0	0
150	0.5511	0.5539	---	---	0.9950	0	0
160	0.5864	0.5866	360.8	0.4391	0.9998	0.7487	0.7486
170	0.5944	0.5968	365.8	0.4640	0.9959	0.7807	0.7775
180	0.5981	0.5975	375.4	0.4934	1.0010	0.8250	0.8258
190	0.6273	0.6300	400.8	0.5269	0.9957	0.8399	0.8363
200	0.6123	0.6102	410.6	0.5509	1.0034	0.8996	0.9027
220	0.6366	0.6316	418.6	0.6035	1.0080	0.9480	0.9556
230	0.6389	0.6377	420.2	0.6292	1.0019	0.9848	0.9867
240	0.6352	0.6315	424.0	0.6626	1.0058	1.0431	1.0492
250	0.6532	0.6503	425.8	0.6820	1.0045	1.0440	1.0487
260	0.6537	0.6480	426.2	0.7159	1.0088	1.0951	1.1048
270	0.6606	0.6575	427.4	0.7268	1.0046	1.1003	1.1054
280	0.6753	0.6675	428.4	0.7625	1.0116	1.1292	1.1423
290	0.6836	0.6798	429.2	0.7751	1.0056	1.1338	1.1401
310	0.6772	0.6683	430.8	0.7920	1.0133	1.1696	1.1852
320	0.6867	0.6816	430.8	0.8082	1.0074	1.1771	1.1858
330	0.6954	0.6852	430.8	0.8310	1.0114	1.1949	1.2127
340	0.6772	0.6696	430.2	0.8188	1.0149	1.2090	1.2228
350	0.6917	0.6817	431.4	0.8393	1.0147	1.2133	1.2311
360	0.7093	0.7043	431.4	0.8548	1.0071	1.2052	1.2137

[a]---, not detectable.

Table S3. Binding energies, XPS spectral deconvolution constraints, and area percent of the deconvoluted bands in each core-level region of the XPS spectra of LM-4-NP and LM-4-NP@Ag.

core-level regions	bands	LM-4-NP				LM-4-NP@Ag				band assignment[b]
		binding energy (eV)	FWHM (eV)	L/G Mix (%) Product	area (%)	binding energy (eV)	FWHM (eV)	L/G Mix (%) Product	area (%)	
C 1s	C_1	284.80	1.49	30	48.3	284.86	1.50	30	45.4	C-C/C=C
	C_2	286.16	1.49	30	32.2	286.11	1.50	30	26.8	C-O/C-OH
	C_3	287.10	1.49	30	17.2	287.07	1.50	30	22.7	O-C-O/C=O
	C_4	288.68	1.49	30	2.2	288.87	1.50	30	5.0	O-C=O
O 1s	O_1	531.73	1.70	30	11.8	531.99	1.70	30	27.0	C=O/C=O*-O
	O_2	533.32	1.70	30	76.0	533.31	1.70	30	66.3	C-O-C/C-OH
	O_3	534.64	1.70	30	12.2	534.41	1.70	30	6.68	C-O
Ag 3d	Ag $3d_{3/2}$	---[a]	---[a]	---[a]	---[a]	374.9	1.68	30	40.0	Ag $3d_{3/2}$
	Ag $3d_{5/2}$	---[a]	---[a]	---[a]	---[a]	368.8	1.68	30	60.0	Ag $3d_{5/2}$

[a]'---' denotes not detectable. [b]the deconvoluted bands were assigned by comparing with the published literature.[3,4]

The calculation of lattice constant (a_0) and average crystallite size (d) of AgNP

The interplanar spacing (d_{hkl}) and lattice constant (a_0) of Ag cubic structure were calculated according to the Bragg's Law (equation (1)) and Miller indices (equation (2)), respectively.[5] In brief, the lattice plane reflections (hkl) = (111), (200), (220), (311) and (222), with the corresponding 2θ = 38.14°, 44.18°, 64.48°, 77.35°, and 81.47°, were used for the calculation of Ag lattice parameter (**Table S4**). The average of the five calculated values of a_0 was compared with the standard a_0 (4.0857 Å) of Ag cubic structure in **Table S4**.[5]

$$d_{hkl} = n\lambda \,/\, 2Sin\theta \quad (1)$$

$$a_0 = d_{hkl}\sqrt{h^2 + k^2 + l^2} \quad (2)$$

d_{hkl} is the interplanar spacing, Å
n is the order of the reflection (integer number), for first-order n=1
λ is the wavelength of the X-ray source, CuKa=1.54184 Å
θ is the Bragg angle in radians (rad)
a_0 is the lattice constant, Å

The average crystallite size (d) of AgNP was calculated following the Scherrer formula (equation (3)),[6,7] which use the full width at half maximum (FWHM) of the major diffraction peak (111).

$$d = K\lambda \,/\, BCos\theta \quad (3)$$

d is the dimension of the crystallite, Å
K is the numerical shape constant, K = 0.89
λ is the wavelength of the X-ray source, CuKa=1.54184 Å
B is the corrected FWHM in radians (rad)
θ is the Bragg angle of the peak maximum in radians (rad)

Table S4. The lattice constant (a_0) of AgNPs calculated from XRD data using the Bragg's Law and Miller indices and compared with the standard a_0 of Ag.

indices			Bragg angle θ (rad)		d-spacing (Å)	lattice constant (Å)	average a_0 (Å)	standard a_0 (JCPD card)	error (%)
					LM-4-NP@Ag-3				
h	k	l	θ	Sinθ	d_{hkl}	a_0	a_0	a_0	a_0
1	1	1	0.3328	0.3267	2.3597	4.0870			
2	0	0	0.3855	0.3760	2.0503	4.1006			
2	2	0	0.5627	0.5334	1.4453	4.0873	4.0910	4.0857	0.13
3	1	1	0.6750	0.6249	1.2337	4.0916			
2	2	2	0.7110	0.6526	1.1813	4.0885			
					LM-4-NP@Ag-5				
h	k	l	θ	Sinθ	d_{hkl}	a_0	a_0	a_0	a_0
1	1	1	0.3326	0.3265	2.3612	4.0895			
2	0	0	0.3853	0.3758	2.0514	4.1028			
2	2	0	0.5626	0.5334	1.4453	4.0873	4.0920	4.0857	0.15
3	1	1	0.6750	0.6249	1.2337	4.0916			
2	2	2	0.7110	0.6526	1.1813	4.0885			
					LM-4-NP@Ag-10				
h	k	l	θ	Sinθ	d_{hkl}	a_0	a_0	a_0	a_0
1	1	1	0.3328	0.3267	2.3597	4.0870			
2	0	0	0.3854	0.3759	2.0509	4.1017			
2	2	0	0.5630	0.5337	1.4445	4.0850	4.0900	4.0857	0.10
3	1	1	0.6757	0.6254	1.2327	4.0883			
2	2	2	0.7112	0.6527	1.1811	4.0879			

Table S5. Comparison of particle size of AgNPs measured from TEM and crystallite size (d) of Ag calculated from XRD pattern using Scherrer formula.

samples	XRD			TEM
	B (rad)	Cosθ	d (nm)	particle size (nm)
LM-4-NP@Ag-3	0.041	0.9451	3.5	8.1 ± 1.2
LM-4-NP@Ag-5	0.039	0.9452	3.7	16.1 ± 1.9
LM-4-NP@Ag-10	0.036	0.9451	4.0	20.7 ± 2.1

Table S6. The XPS results in atomic%.

sample	C 1s	O 1s	Ag 3d
LM-4-NP	77.9	22.1	0
LM-4-NP@Ag	75.1	21.5	3.4

Table. S7 Mass-based metrics for evaluating "greenness" in LNP@Ag preparation.

samples	mass input (mg)		reaction time (hours)	product (mg)	yield (%)[c]	waste (mg)	mass-based metrics	
	LNP[a]	$Ag(HN_3)_2NO_3$[b]		LNP@Ag	LNP@Ag	$Ag(HN_3)_2NO_3$[d]	reaction mass efficiency[e] (%)	E factor[f]
LM-4-NP@Ag-3	16	12	4	17.4	109	7.4	62	0.42
LM-4-NP@Ag-5	16	20	4	23.0	143	9.8	64	0.43
LM-4-NP@Ag-10	16	40	4	24.2	150	28.6	43	1.18
LM-4-NP@Ag-10*	16	40	6	23.0	144	29.8	41	1.29

[a]2 mL LNP dispersion; [b]4 mL $Ag(NH_3)_2NO_3$ solution, ignore the weight of $NH_3.H_2O$; [c]yield (%) = 100 x $m_{(LNP@Ag)}$ (recovered by centrifugation and freeze-drying) / $m_{(LNP)}$ fed initially;
[d]waste $Ag(NH_3)_2NO_3$ = mass input $Ag(NH_3)_2NO_3$ – (mass of Ag^+ reduced to metallic Ag), ignore the weight of $NH_3.H_2O$
[e]reaction mass efficiency = 100 x mass of product (LNP@Ag) / mass of total input
[f]E(nvironmental) factor = total waste/mass of product (LNP@Ag)

Table S8. Comparison of the antimicrobial activity of as-prepared GGMMA/LNP@Ag hydrogel with other hydrogel or film that engaged lignin-capped AgNPs as the antimicrobial component.

materials	loading of [lignin-Ag]-based sample (wt%)	antibacterial testing		bactericidal ratio (%)					Ref.
		testing approach	testing time (h)	*P. aeruginosa*	*E. coli*	*S. aureus*	*S. epidermidis*	*L. monocylogenes*	
GGMMA-LNP@Ag hydrogel	0.10	colony-counting method	4	---[a]	99	99	---	---	**this work**
polyurethane-[lignin-AgNP] foam	0.12		24	99	---	90	---	---	8
poly(vinyl alcohol)-[lignin-AgNP] hydrogel	14		24	---	99	99	---	---	9
poly(lactide)-[lignin-AgNP] film	1.00		3	---	100	---	---	99	10
polyacrylic acid-pectin-[lignin-AgNP] hydrogel	> 0.08	optical density	24	---	97	---	98	---	11
agar-[lignin-AgNP] film	1.00		3	---	99	---	---	37 (6 h, 99%)	12

[a]'---' the strain was not included in the antimicrobial experiment.

Table S9. The yield of laccase-polymerized lignin from birch AL fractions and LNP as well as LNP@Ag yield obtained from laccase-polymerized lignin.

lignin fractions	laccase-catalyzed polymerization			LNP preparation				LNP@Ag preparation[c]		
	initial weight (mg)	isolated weight (mg)	yield[a] (%)	initial weight (mg)	insoluble fraction (mg)	LNP (mg)	yield[b] (%)	initial weight (mg)	LNP@Ag obtained (mg)	yield[d] (%)
birch AL	210	218	109	100	9	82	82	16	20	126
birch-*i*-PrOH-s	209	205	102	100	9	79	79	16	14	88
birch-EtOH-s	205	208	102	100	2	71	71	16	18	112
birch-MeOH-s	200	204	102	100	8	81	81	16	24	150

[a]calculated after 4 hours incubation with laccase, yield (%) = 100 x $m_{(laccase\text{-}polymerized\ lignin)}$ (recovered by acid precipitation, centrifugation, and freeze-drying) / $m_{(lignin\ fraction)}$ fed initially

[b]yield (%) = 100 x $m_{(LNP)}$ (recovered by centrifugation and freeze-drying) / $m_{(laccase\text{-}polymerized\ lignin)}$ fed initially

[c]the LNP@Ag was prepared by impregnating LNP in $Ag(NH_3)_2NO_3$ solution (10 $mg.mL^{-1}$) for 4 hours

[d]yield (%) = 100 x $m_{(LNP@Ag)}$ (recovered by centrifugation and freeze-drying) / $m_{(LNP)}$ fed initially

References

1 S. Piqueras, S. Füchtner, R. Rocha de Oliveira, A. Gómez-Sánchez, S. Jelavić, T. Keplinger, A. de Juan and L. G. Thygesen, *Front. Plant Sci.*, 2020, **10**, 1–15.

2 C. G. Boeriu, D. Bravo, R. J. A. Gosselink and J. E. G. Van Dam, *Ind. Crops Prod.*, 2004, **20**, 205–218.

3 L. Zhang, H. Lu, J. Chu, J. Ma, Y. Fan, Z. Wang and Y. Ni, *ACS Sustain. Chem. Eng*., 2020, **8**, 12655–12663.

4 Z. Tian, L. Zong, R. Niu, X. Wang, Y. Li and S. Ai, *J. Appl. Polym. Sci*, 2015, **132**, 42057.

5 B. K. Mehta, M. Chhajlani and B. D. Shrivastava, *J. Phys. Conf. Ser.*, 2017, **836**, 012050.

6 K. He, N. Chen, C. Wang, L. Wei and J. Chen, *Cryst. Res. Technol.*, 2018, **53**, 1–6.

7 S. Chen, G. Wang, W. Sui, A. M. Parvez and C. Si, *Green Chem.*, 2020, **22**, 2879–2888.

8 A. G. Morena, I. Stefanov, K. Ivanova, S. Pérez-Rafael, M. Sánchez-Soto and T. Tzanov, *Ind. Eng. Chem. Res.*, 2020, **59**, 4504–4514.

9 M. Li, X. Jiang, D. Wang, Z. Xu and M. Yang, *Colloids Surf. B: Biointerfaces*, 2019, **177**, 370–376.

10 S. Shankar, J. W. Rhim and K. Won, *Int. J. Biol. Macromol.*, 2018, **107**, 1724–1731.

11 D. Gan, W. Xing, L. Jiang, J. Fang, C. Zhao, F. Ren, L. Fang, K. Wang and X. Lu, *Nat. Commun.*, 2019, **10**, 1–10.

12 S. Shankar and J. W. Rhim, *Food Hydrocoll.*, 2017, **71**, 76–84.